Angle-Resolved Cathodoluminescence Imaging Polarimetry
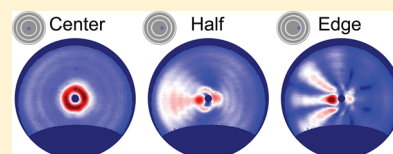
Clara I. Osorio,[†] Toon Coenen,[†] Benjamin J. M. Brenny,[†] Albert Polman, and A. Femius Koenderink*

Center for Nanophotonics, FOM Institute AMOLF, Science Park 104, 1098 XG Amsterdam, The Netherlands

S *Supporting Information*

ABSTRACT: Cathodoluminescence spectroscopy (CL) allows characterizing light emission in bulk and nanostructured materials and is a key tool in fields ranging from materials science to nanophotonics. Previously, CL measurements focused on the spectral content and angular distribution of emission, while the polarization was not fully determined. Here we demonstrate a technique to access the full polarization state of the cathodoluminescence emission, that is the Stokes parameters as a function of the emission angle. Using this technique, we measure the emission of metallic bullseye nanostructures and show that the handedness of the structure as well as nanoscale changes in excitation position induce large changes in polarization ellipticity and helicity. Furthermore, by exploiting the ability of polarimetry to distinguish polarized from unpolarized light, we quantify the contributions of different types of coherent and incoherent radiation to the emission of a gold surface, silicon and gallium arsenide bulk semiconductors. This technique paves the way for in-depth analysis of the emission mechanisms of nanostructured devices as well as macroscopic media.

KEYWORDS: *cathodoluminescence, polarimetry, transition radiation, plasmonic antennas, nanospirals*

Among many recent developments in microscopy, optical electron-beam spectroscopy techniques such as cathodo-luminescence imaging (CL) have emerged as powerful probes to characterize materials and nanophotonic structures and devices. In CL, one collects light emitted in response to a beam of energetic electrons (0.1−30 keV), for example in a scanning electron microscope (SEM). The time-varying evanescent electric field around the electron beam interacts with polarizable matter creating coherent emission, such as surface plasmon polaritons (SPP) and transition radiation (TR).[1−3] The spot size of the focused electron beam and the extent of the evanescent field about the electron trajectory define the interaction resolution to be below ∼20 nm. A broadband excitation results from the interaction time (approximately 1 fs) set by the high velocity of each electron due to its high energy. Aside from coherent emission, incoherent emission can also be generated both by the primary beam and by slower secondary electrons, which excite electronic transitions in matter.[3,4] The relative importance of the coherent and incoherent contributions provides information about the material composition and electronic structure. Spectral analysis of the cathodolumines-cence as a function of the electron beam position allows the local characterization of the structure and defects of semi-conductors,[5−7] the functioning of nanophotonic devices,[8] and mapping the plasmonic resonances of plasmonic and metamaterial structures.[9] Recently developed techniques for detection of CL enable the identification of the band structure and Bloch modes of photonic crystals,[1,10−13] the dispersion of surface plasmons,[2,14] and the directivity and Purcell enhance-ment of plasmonic nanoantennas.[15,16]

Besides frequency and linear momentum, the vectorial nature of light provides a third degree of freedom rich in information about the physics of light generation and scattering, encoded in the polarization of emitted light. In materials characterization, for instance, polarization gives direct access to the local orientation of emission centers and anisotropies in the host material. In nanophotonics, polarization plays a fundamental role (together with directionality) in determining the interaction between emitters and nanostructures. Furthermore, it is increasingly recognized that mapping and controlling the polarization of light is key to harnessing the wide range of opportunities offered by metamaterials and metasurfaces. Recent breakthroughs in chirality-enhanced antennas,[17] pho-tonic topological insulators,[18] and the photonic equivalent of the spin-Hall effect[19−22] indicate the emerging importance of mapping the full polarization properties of nanophotonic structures. Polarization measurements of CL emission, however, have been limited to fully polarized emission and, in particular, to linearly polarized signals.[23,24]

In this Article, we introduce a novel technique to access full polarization information in cathodoluminescence spectroscopy. Based on a polarization analysis method previously demon-strated in optical microscopes,[25−28] we integrate a rotating-plate polarimeter in the detection path of the angle-resolved CL setup. Using the Mueller matrix formalism for the light collection system, we determine the Stokes parameters for CL emission, that is, all parameters required to completely describe the polarization state of the light, which can be polarized, partially polarized, or totally unpolarized. We demonstrate the great potential of this new measurement technique by analyzing the angle-resolved polarization state of directional plasmonic bullseye and spiral antennas. Further-more, and exploiting the unique capabilities of CL excitation, we measured the emission from metals and semiconductors. For these materials, we can separate coherent and incoherent
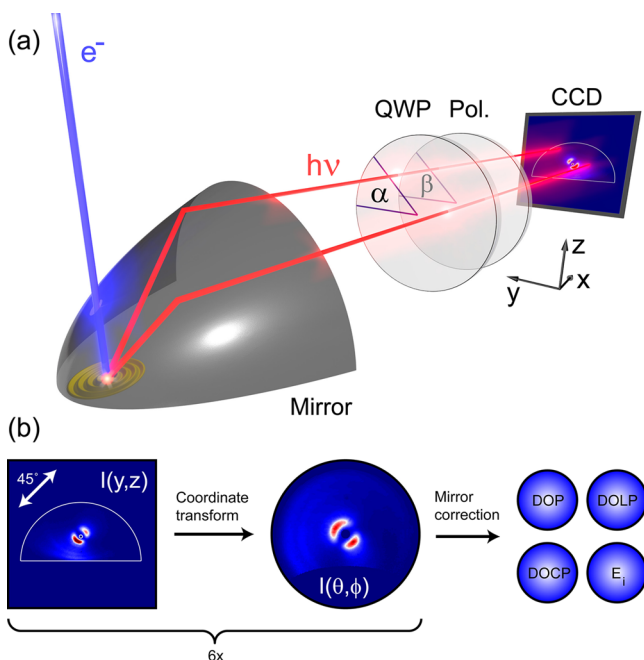
emission mechanisms, with further applications in nanoscale materials science.

■ CL POLARIMETRY

In our measurements, the 30 keV electron beam from a scanning electron microscope (SEM) excites the sample. An aluminum paraboloid mirror collects and redirects the resulting CL emission out of the SEM. The outcoming beam is focused onto a fiber-coupled spectrometer or projected onto a 2D CCD array,[13,15,29] as shown in Figure 1a. The wave-vector

(a)

(b)

Figure 1. (a) Schematic overview of the cathodoluminescence polarimetry setup. The structure is excited by the electron beam after which the resulting light emission is collected by a parabolic mirror. The light is directed toward a polarimeter composed of a QWP and linear polarizer set at angles α and β, respectively. The filtered beam profile is measured by the CCD camera. The CCD images shows data corresponding to a measurement on a bullseye structure with $\alpha = \beta = 45°$. For reference we also show the coordinate system that is used throughout the manuscript. (b) Six measurements with different settings of the polarimeter are required to retrieve the full angle-resolved polarization state of the collected light. In addition to transforming from Cartesian (y,z) coordinates in the detection plane to polar coordinates (zenithal angle θ, azimuthal angle φ) in the emission plane, we corrected for the effect of the mirror on the polarization. Using the retrieved Stokes parameters it is possible to determine any figure of merit for polarization including the total (DOP), linear (DOLP), and circular (DOCP) degrees of polarization, as well as the electric field components $|E_i|$.

distribution of the CL emission can be retrieved from the CCD image, as every transverse point in the beam corresponds to a unique emission angle, in a procedure analogous to other Fourier imaging techniques.[30−35]

Measuring polarization for all emission angles of CL presents several challenges. First, it requires determining the relative phase difference between field components, a task not achievable with only linear polarizers, as in ref 23. Second, the paraboloid mirror performs a nontrivial transformation on the signal as it propagates from the sample to the detector plane. The shape of the mirror introduces a rotation of the

vector components of light due to the coordinate transformation and, consequently, a change in the main polarization axes. In addition, the angle and polarization-dependent Fresnel coefficients of the mirror modify the polarization of the light upon reflection.[36,37] As a function of the angle of incidence, the mirror partially polarizes unpolarized light and transforms linearly to elliptically polarized light.

To address these challenges, we included a rotating-plate polarimeter in the beam path of our CL system, composed of a quarter wave plate (QWP) and a linear polarizer.[38−40] Figure 1a shows the polarizing elements in a schematic of the setup. Depending on their orientation, these two elements act either as a linear polarizer or as a right or left handed circular polarizer. As shown in Figure 1b, we measure the intensities I_j transmitted by six different settings of the polarimeter (horizontal, vertical, 45°, 135°, right- and left-handed circular) in order to determine the Stokes parameters of the light:
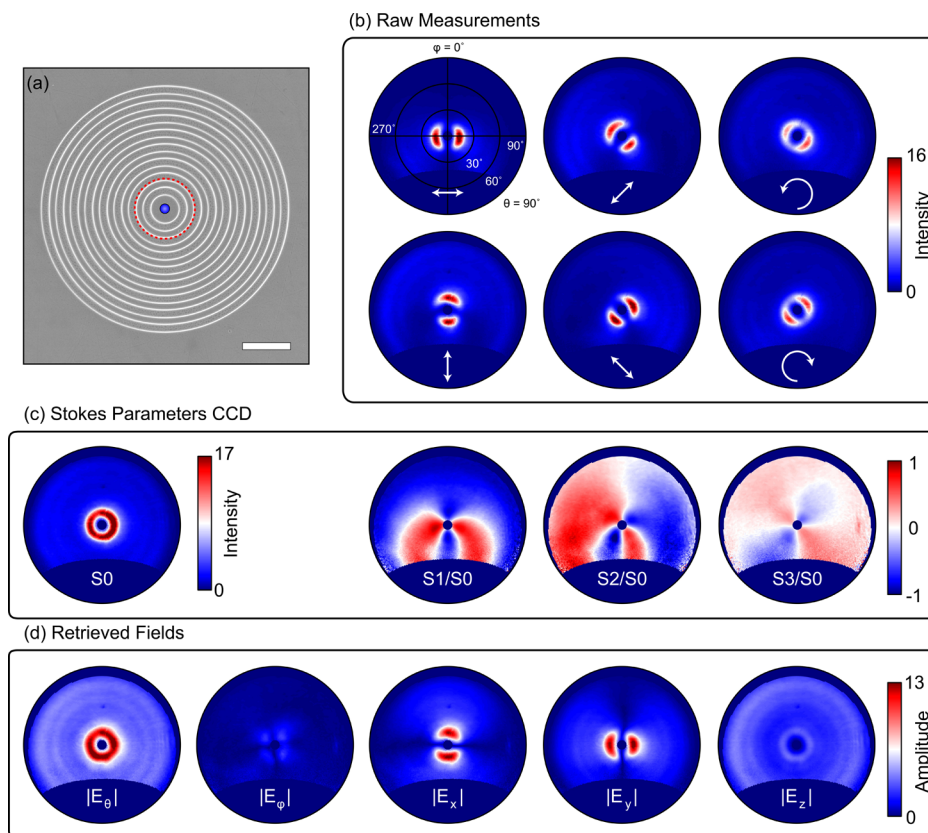
$$
\begin{aligned}
S_0 &= I_H + I_V \\
S_1 &= I_H - I_V \\
S_2 &= I_{45} - I_{135} \\
S_3 &= I_{RHC} - I_{LHC}
\end{aligned}
\tag{1}
$$

These four parameters are the most general representation of polarization and can be used to retrieve any polarization-related quantity.[39] The raw polarization-filtered CCD images are projected onto $[\theta, \varphi]$-space, as indicated in Figure 1b using a ray-tracing analysis of the mirror, after which the Stokes parameters in the detection plane are determined. To transform these to Stokes parameters in the sample plane, we determine the Mueller matrix of the light collection system that accounts for the effects of the mirror on the polarization. In addition to the geometrical transformation, the analysis takes into account the Fresnel coefficients of the mirror for s- and p- polarized light. Due to the 3D shape of the mirror, each element of the Mueller matrix is a function of the emission angle, that is, there is a Mueller matrix for each emission angle. The Supporting Information describes in more detail how the Mueller matrix was calculated. To benchmark these calculations, we use fully polarized transition radiation (TR) which occurs whenever an electron traverses an interface between two dielectric media. The electron locally polarizes the material close to the interface, giving rise to a well-defined broadband vertically oriented point-dipole-like source,[3,23,29] which is perfectly suited to calibrate our CL polarimeter (see Figure S2).

The Stokes parameters in the sample plane allow determining *any* figure of merit for polarization. Given that both incoherent and coherent radiation may be generated in CL, the degree of polarization (DOP), and the degrees of linear (DOLP) and circular (DOCP) polarization will be especially relevant. Defined as the ratios of polarized, linearly polarized, or circularly polarized light to total intensity, they are given by

$$
\mathrm{DOP} = \sqrt{S_1^2 + S_2^2 + S_3^2}/S_0, \quad \mathrm{DOLP} = \sqrt{S_1^2 + S_2^2}/S_0 \quad \text{and}
$$

$\mathrm{DOCP} = S_3/S_0$. Equivalently, the ratio of unpolarized light to total intensity is given by $1 - \mathrm{DOP}$, so a DOP smaller than 1 corresponds to partially polarized light.

■ CL POLARIMETRY ON PLASMONIC STRUCTURES

Bullseye Antennas. To demonstrate the full potential of angle-resolved CL polarimetry, we investigate the emission of a plasmonic bullseye structure with a pitch $d = 600$ nm, milled

Figure 2. (a) Scanning electron micrograph of a bullseye structure with d = 600 nm. The blue dot indicates the electron beam excitation position. The red dashed circle indicates which part of the bullseye is shown in detail in Figure 3. The scale bar corresponds to 2 μm. (b) Polarization filtered angular CL patterns for different analyzer settings as indicated by the white arrows, measured at λ_0 = 750 nm. (c) Stokes parameters in the detection plane as a function of angle. The S_1, S_2, and S_3 patterns are normalized to S_0 to better show the overall polarization distribution. (d) Spherical and Cartesian field amplitude distributions as a function of angle, retrieved from the experimental data in (b). In all figures, the intensities are given in 10^5 ADU sr^{-1}s^{-1}. Amplitudes are in units of $10^2 \sqrt{\text{ADU sr}^{-1} \text{ s}^{-1}}$ (analog-to-digital units).

into a single-crystal gold substrate. Bullseyes are well-known for their ability to strongly direct light scattered by nanoscale apertures,[41] generated by fluorescence[33,42] or thermal emission.[43] Figure 2a shows a scanning electron micrograph of the structure indicating the excitation position. The electron beam launches a circular surface plasmon polariton (SPP) wave that radiates outward and scatters coherently from the grooves of the bullseye. The scattered fields interfere to give rise to directional emission. In our measurements, the emission is spectrally filtered by a 40 nm bandwidth bandpass filter centered at λ_0 = 750 nm (see Figure S1 in the supplement for full spatial and spectral mapping).

Figure 2b−d represent the main steps of our polarimetric analysis for CL. Figure 2b shows the angular intensity patterns measured for the six settings of the polarimeter (indicated by the arrows) after a coordinate transformation of the raw intensity data. Figure 2c shows the Stokes parameters in the detection plane calculated using eq 1 from the patterns in Figure 2b. The leftmost panel corresponds to the total intensity distribution, S_0. The bullseye emits in a narrow doughnut pattern without any azimuthal variations, consistent with the azimuthal symmetry of both excitation position and bullseye structure. The polar angle at which most of the CL is emitted, θ = 15°, corresponds to the grating equation $\theta = \sin^{-1}(k_{\text{SPP}} - m2\pi/d)/k_0$. In this spectral regime, the grating order m = 1 is the only relevant order, $k_0 = 2\pi/\lambda_0$ and k_{SPP} is the SPP wavevector, calculated using the optical constants for gold from
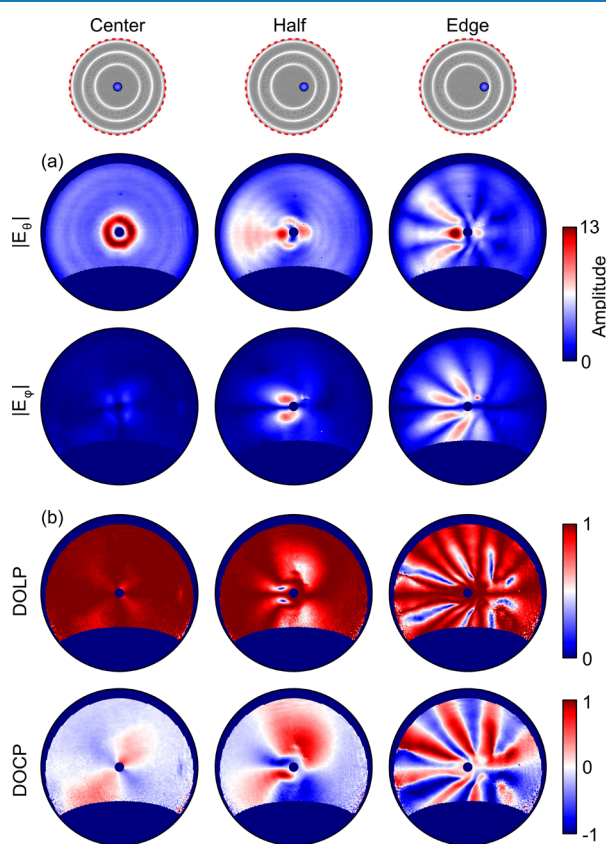
spectroscopic ellipsometry. The other panels in Figure 2c show the Stokes parameters S_1, S_2, and S_3 in the detection plane (yz-plane in Figure 1) normalized to S_0, such that it is possible to see polarization features outside the areas of very bright emission.

Next, we transform the data collected by the detector to the polarization state of the emitted light in the sample plane, by multiplying the Stokes parameters at the detection plane with the mirror's inverse Mueller matrix. Among the quantities that the Stokes parameters allow retrieving, here we will focus on the electric field components. Figure 2d shows the reconstructed spherical field vector amplitudes $|E_\varphi|$ and $|E_\theta|$ that constitute the natural s- and p- polarization basis relevant to map the far-field generated by a localized radiating object. The figure shows that the $|E_\theta|$ distribution is strong and azimuthally symmetric, while $|E_\varphi|$ is close to zero. Therefore, the measured emission of the bullseye is a narrow doughnut beam with a fully linear, radial polarization. Radial polarization is expected for the bulls-eye radiation as SPPs scatter out while maintaining their p-polarized character at the grooves.

The polarization can alternatively be cast into Cartesian components. Figure 2d shows the double-lobe patterns of $|E_x|$ and $|E_y|$, which are rotated 90° relative to each other. The $|E_z|$ component is azimuthally symmetric and shows several emission rings. The outer rings correspond to transition radiation (TR) from the excitation position, which is modulated to yield a fringe pattern due to interference with

SPPs scattered off the bullseye grooves. This interference in the far field results from the fact that both TR and SPPs are coherent radiation excited by the same source (same electron).[3,44] Since the electric field must be transverse to the propagation direction, the $|E_z|$ component vanishes at near-normal angles, and therefore, the main SPP emission beam from the bullseye (the narrow ring) appears relatively weak in $|E_z|$. While the emission in the sample plane is completely linearly polarized, a nonzero circular polarized signal is measured in the detection plane (S_3 in Figure 2c), which indicates the effect of the mirror and the importance of using the Mueller matrix analysis to correct for it.

Nonsymmetric Geometries. CL polarimetry is a unique tool to explore the relation between the symmetry of a system and its polarization response. While the symmetry of a bullseye structure excited right at the center ensures the clear TM polarization emission shown in Figure 2d, this is no longer the case when launching an off-center circular SPP wave on the structure. Figure 3 shows measurements for electron beam

Figure 3. (a) $|E_\theta|$ and $|E_\varphi|$ field amplitudes for central, halfway, and edge excitation on the bullseye plateau. The excitation positions are indicated as blue circles in the SEM micrographs on top, which show the area enclosed by the red dashed circle in Figure 2a. (b) Degree of linear (DOLP) and circular (DOCP) polarization of the bullseye emission as a function of emission angle for the same excitation positions as in (a).

excitation in the center, halfway between the center and the edge, and at the edge of the central bullseye plateau, as indicated in the SEM micrographs on top of the figure. Figure 3a shows $|E_\theta|$ and $|E_\varphi|$ for the three excitation positions. For off-center excitation, the zenithal field distribution $|E_\theta|$ is no longer symmetric, being stronger toward the left than toward the right
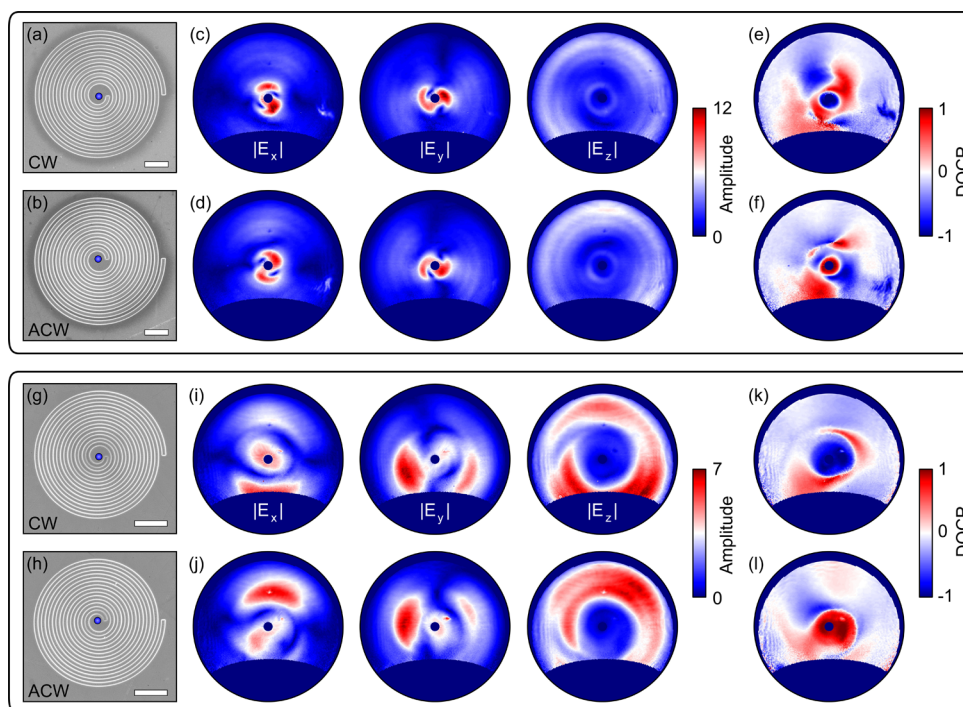
of the image. This type of asymmetric beaming has also been observed in angular intensity measurements on asymmetric gratings,[42] spirals,[45] and asymmetrically excited (patch) antennas.[24,46] Besides the asymmetry, the off-center excitation also leads to a nonzero azimuthal field contribution, $|E_\varphi|$, which is similar in strength to the zenithal field contribution. The excitation position and the center of the bullseye defines a mirror symmetry that expresses itself as a nodal line for $|E_\varphi|$ at $\varphi = 90°$ and $270°$. At far off-center excitation, the azimuthal and zenithal field distributions are very rich in structure, and for certain angular ranges, the emission becomes elliptically or circularly polarized.

The effect of off-center excitation is most clearly seen in Figure 3b, which shows the degree of linear (DOLP) and circular (DOCP) polarization. Owing to the mirror symmetry of the sample and the excitation, the DOCP remains close to zero along the axis of the electron beam displacement. Yet, away from this axis, the emission becomes elliptical with opposite handedness on either side of the axis, as dictated by mirror symmetry. For edge excitation, the complementary multilobe $|E_\theta|$ and $|E_\varphi|$ patterns lead to a rich behavior, where the emission changes from fully linear to almost fully circular polarization several times.

Rather than breaking symmetry by changing the excitation position, it is also possible to study scattering and emission by intrinsic asymmetry and handedness of structures such as Archimedean spirals. Spirals enjoy a growing interest since it was shown that they can enhance the extraordinary transmission of single nanoapertures for particular helicities[47] and transfer polarization and orbital angular momentum to scattered photons.[45,48] This can result in a polarization-dependent directional beaming[49] and demonstrates strong photon spin−orbit coupling effects.[17]

We fabricated Archimedean spiral gratings with clockwise (CW) and anticlockwise (ACW) orientation, as shown in Figure 4a,b, and used CL polarimetry to study the effect of spiral asymmetry and handedness on the far-field polarization, again taking a pitch $d = 600$ nm and $\lambda_0 = 750$ nm. We excite the spirals in their origin as indicated in Figure 4. Figure 4c,d shows the Cartesian components of the far-field emission of the spirals, which better reflect the handedness than the spherical fields. Since the groove pitch is the same for spirals and bullseyes, the angular spread of these patterns is similar. However, the emission by the spirals does not have a minimum around the region excluded by the mirror hole ($\theta = 0$) and the s-like shape in $|E_x|$ and $|E_y|$ clearly reflects their handedness.

In contrast with bullseyes excited at their center, the spirals can induce ellipticity in the polarization of the light even when excited in their origin, as shown in Figure 4e,f. This is particularly evident in the region of higher intensity in the vicinity of the normal, where the DOCP is close to ± 1. Thereby, the spirals are highly directional sources of circularly polarized light. Mirrored spirals simply exhibit mirrored patterns (where the y-axis defines the mirror symmetry), conserving intensities and field strengths, while the sign of the DOCP changes. This result indicates that swapping spiral handedness not only flips the helicity of the output field but, in addition, it mirrors the distribution of intensity over angle. For spirals with smaller pitch, we find similar but even stronger effects of handedness, aided by the fact that their radiation pattern is more strongly off-normal (see Figure 4g−l). In that case, the $|E_z|$ distribution is also clearly chiral.

Figure 4. Scanning electron micrographs of (a) a clockwise (CW) and (b) anticlockwise (ACW) Archimedean spiral grating with $d = 600$ nm. Amplitude distributions of the Cartesian fields for (c) a CW spiral and (d) a ACW spiral. Degree of circular polarization (DOCP) for (e) a CW spiral and (f) an ACW spiral. Scanning electron micrographs of (g) a CW and (h) ACW spiral with $d = 440$ nm. Amplitude distributions of the Cartesian fields for (i) a CW spiral and (j) a ACW spiral. DOCP for (k) a CW spiral and (l) an ACW spiral. All measurements were performed at $\lambda_0 = 750$ nm. For reference, we again indicate the electron beam excitation position with a blue dot. Scale bars in the electron micrographs correspond to 2 μm.

The data shown in this section proves that polarimetry analysis of CL, in combination with precise electron beam positioning, provides direct insight into the complex emission behavior of nanophotonic structures. Measuring directionality and polarization of the emission from emitters coupled to single nanostructures is of paramount importance when designing and testing the performance of structures like optical antennas, plasmonic resonators, and metasurfaces.

CL POLARIMETRY APPLIED TO INCOHERENT EMITTERS

In addition to characterizing fully coherent radiation, CL polarimetry allows us to determine whether the measured radiation contains an unpolarized contribution such as in the case of incoherent luminescence from bulk or nanostructured materials. This is shown in Figure 5, where we compare azimuthally averaged zenithal cross cuts of the polarized ($S_0 \times$ DOP) and unpolarized ($S_0 \times (1 - \text{DOP})$) emission intensities for single-crystal, unpatterned Au, Si, and GaAs and compare them to calculations.
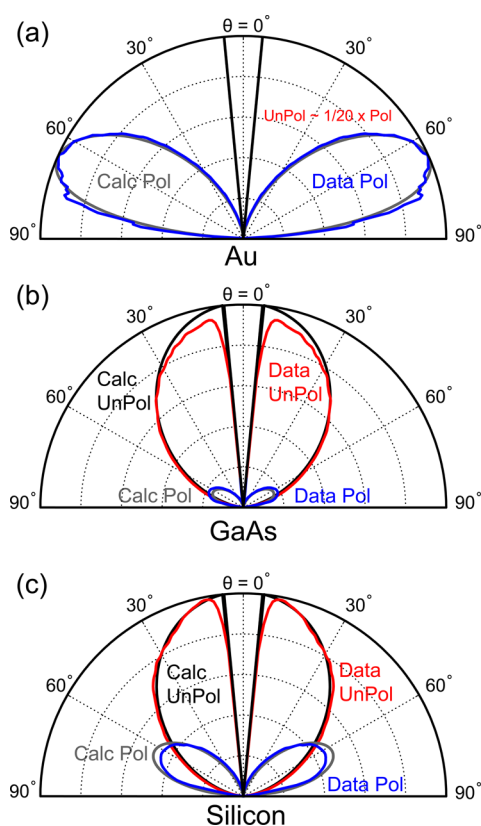
The emission from Au is dominated by TR, which is fully coherent and polarized radiation. Figure 5a shows a measurement at $\lambda_0 = 850$ nm, which completely overlaps with a calculated TR emission distribution (see also Figure S2 in the supplement). In the case of GaAs in Figure 5b, the emission is dominated by very bright incoherent radiative band-to-band recombination measured at $\lambda_0 = 850$ nm. This luminescence is fully isotropic and unpolarized *inside* the material, but large differences between *s*- and *p*-Fresnel transmission coefficients for the semiconductor–vacuum interface partially polarize the emission, as seen in the data. Figure 5b shows that unpolarized light is indeed dominant. The weak polarized emission has a

very different angular emission distribution, that agrees well with Fresnel calculations (see Figure S3 in the supplement for more information). Lastly, Si is a material that displays weak luminescence that it is comparable to TR.[50] Indeed, the polarized intensity for Si at $\lambda_0 = 650$ nm shown in Figure 5c constitutes ~31.7% of the total emission, which is much more significant than for GaAs, although unpolarized emission remains the dominating contribution.

These examples show that angle-resolved polarimetry measurements provide quantitative and precise information about the origin of emission of different materials. This technique enables the separation of polarized and unpolarized emission, and therefore it can be used to determine the different mechanisms that simultaneously contribute to cathodoluminescence (see Figure S2 in the supplement for a quantitative analysis of TR). Moreover, for the polarized part of the emission we can map the electric field components and their relative phase. Since it does not require any prior knowledge of the sample (unlike the method described in ref 50), this method is very general and can be applied to any (nanostructured) material.

CONCLUSION

We have demonstrated "angle-resolved cathodoluminescence imaging polarimetry" as a new microscopy tool to map the vectorial electromagnetic scattering properties of nanostructured and bulk materials. We determine the complete polarization state of emitted light as a function of angle from six CL intensity measurements in the detection plane, in combination with a mathematical transformation that corrects for the polarizing effect of the CL mirror. Due to the high resolution of the electron beam excitation, the wave-vector

Figure 5. Zenithal cross cuts comparing unpolarized and polarized emission for bulk single crystals of Au at $\lambda_0 = 850$ nm (a), GaAs at $\lambda_0 = 850$ nm (b), and Si at $\lambda_0 = 650$ nm (c). In all cases we compare the unpolarized (red) and polarized (blue) emission from measurements to the unpolarized (black) and polarized (gray) emission determined from calculations. The data is obtained by averaging over an azimuthal range $\varphi = 270-90°$ to improve signal-to-noise ratio, and we scale the angular distributions by the overall emission intensity. For Au, the unpolarized emission component is so small that it is not visible in the plot.

resolved polarization properties of locally excited plasmonic nanoantennas can be extracted with a spatial resolution for the excitation of 20 nm. The angle-resolved polarization measurements of the emission of bullseye and spiral nanoantennas demonstrate how structural symmetry and handedness translate into the helicity of emitted light. These results show that angle-resolved cathodoluminescence polarimetry can be extremely valuable for the development of metallic and dielectric antennas for spin-resolved and chiral spectroscopy as well as for the study of photon spin Hall effects.

Besides its relevance for nanophotonics, we demonstrate that our technique opens new perspectives for materials science not accessible with optical microscopes. Measuring the Stokes parameters generally enables the separation of incoherent and coherent CL generation, as we demonstrated for direct and indirect semiconductor materials. Our measurements on relatively simple samples of Au, GaAs, and Si show the potential of the technique for the analysis of bulk materials which could be useful for many material inspection tasks. For optoelectronics, the nanoscale characterization of emission polarization from inorganic LEDs stacks, nanowires, and quantum dots stands out in particular. The technique also introduces the possibility of locally studying material anisotropy, birefringence, and optical activity.

METHODS

Sample Fabrication. We fabricated bullseye and spiral structures by patterning a single-crystal Czochralski-grown Au ⟨100⟩ pellet, which was mechanically polished to obtain a sub-10 nm RMS roughness. The patterning was done by using a 30 keV Ga$^+$ ion beam in a FEI Helios NanoLab dual beam system at 9.7 pA beam current and a dwell time of 10 μs per pixel. In the bullseye design the central plateau has a diameter of 1.2 μm (2× the pitch, 600 nm) and the duty cycle of the circular grating consisting of eight grooves is 50%. The spiral design is based on an Archimedean spiral, where the first half period of the spiral is omitted. For the spiral, we show data both for 600 and 440 nm pitches. Both for the spirals and the bullseyes, the groove depth was ∼110 nm. The measurements on silicon were performed on a polished p-type (boron doping level $10^{15}-10^{16}$ cm^{-3}) single-crystal ⟨100⟩ wafer. The measurements on GaAs were done on a polished single-crystal ⟨100⟩ wafer.

Measurements. The measurements were performed in a FEI XL-30 SFEG (30 keV electron beam, 30 nA current) equipped with a home-built CL system.[13,15,29] To obtain the polarization state of the emission, we perform a series of six measurement of the angular CL pattern using a 2D back-illuminated CCD array. Each measurement was taken with a different setting of the polarimeter, defined by a specific combination of QWP and polarizer angles. Handedness of circularly polarized light was defined from the point of the view of the source, following the IEEE standard. In this case, right-handed circularly polarized light rotates anticlockwise and left-handed circularly polarized light rotates clockwise. We use the known transition radiation pattern from an Au surface to calibrate the optical detection system. A 40 nm band-pass color filter spectrally selected the measured emission. For the bullseye and spiral measurements we used 30 s integration time, which is a good compromise between a small spatial drift of the electron beam and a good signal-to-noise in CL. For the TR emission from single-crystal gold and the measurements on silicon we used 120 s integration time since TR emission and luminescence are position independent and the measurement is not affected by spatial drift of the electron beam. For the measurements on GaAs we used a much lower current (0.9 nA) and integration time (1 s) due to the very bright band gap luminescence. For every setting of the polarimeter, we collected a dark reference measurement where we blank the electron beam (with the same integration time as the CL measurement), which was subtracted from the data in the postprocessing stage. Possible sources of errors on the measurements include e-beam drift (in the case of position dependent samples), bleaching/contamination during measurements leading to a reduction in CL signal, fluctuations in current and mirror alignment.

ASSOCIATED CONTENT

ⓈSupporting Information

The Supporting Information is available free of charge on the ACS Publications website at DOI: 10.1021/acsphotonics.5b00596.

    Further information about the calculation of the Mueller matrix, the calibration of set-up, the spectral response of the antennas, and the data analysis for the bulk material measurements (PDF).

AUTHOR INFORMATION

Corresponding Author
*E-mail: f.koenderink@amolf.nl.

Author Contributions
†These authors contributed equally to this work (C.I.O., T.C., and B.J.M.B.).

Notes
The authors declare the following competing financial interest(s): Albert Polman is co-founder and co-owner of Delmic BV, a startup company that develops a commercial product based on the ARCIS cathodoluminescence system that was used in this work.

REFERENCES

(1) Adamo, G.; Ou, J. Y.; So, J. S.; Jenkins, S. D.; De Angelis, F.; MacDonald, K. F.; Di Fabrizio, E.; Ruostekoski, J.; Zheludev, N. I. Electron-Beam-Driven Collective-Mode Metamaterial Light Source. *Phys. Rev. Lett.* **2012**, *109*, 217401.

(2) Bashevoy, M. V.; Jonsson, F.; MacDonald, K. F.; Chen, Y.; Zheludev, N. I. Hyperspectral imaging of plasmonic nanostructures with nanoscale resolution. *Opt. Express* **2007**, *15*, 11313–11320.

(3) García de Abajo, F. J. Optical excitations in electron microscopy. *Rev. Mod. Phys.* **2010**, *82*, 209–275.

(4) Yacobi, B. G.; Holt, D. B. *Cathodoluminescence Microscopy of Inorganic Solids*; Springer, 1990.

(5) Edwards, P. R.; Martin, R. W. Cathodoluminescence nano-characterization of semiconductors. *Semicond. Sci. Technol.* **2011**, *26*, 064005.

(6) Sauer, R.; Sternschulte, H.; Wahl, S.; Thonke, K.; Anthony, T. R. Revised Fine Splitting of Excitons in Diamond. *Phys. Rev. Lett.* **2000**, *84*, 4172–4175.

(7) Ton-That, C.; Weston, L.; Phillips, M. Characteristics of point defects in the green luminescence from Zn- and O-rich ZnO. *Phys. Rev. B: Condens. Matter Mater. Phys.* **2012**, *86*, 115205.

(8) Spirkoska, D.; et al. Structural and optical properties of high quality zinc-blende/wurtzite GaAs nanowire heterostructures. *Phys. Rev. B: Condens. Matter Mater. Phys.* **2009**, *80*, 245325.

(9) Zhu, X. L.; Ma, J. S.; Zhang, Y.; Xu, X. F.; Wu, J.; Zhang, Y.; Han, X. B.; Fu, Q.; Liao, Z. M.; Chen, L.; Yu, D. P. Confined three-dimensional plasmon modes inside a ring-shaped nanocavity on a silver film imaged by cathodoluminescence microscopy. *Phys. Rev. Lett.* **2010**, *105*, 127402.

(10) Suzuki, T.; Yamamoto, N. Cathodoluminescent spectroscopic imaging of surface plasmon polaritons in a 1-dimensional plasmonic crystal. *Opt. Express* **2009**, *17*, 23664–23671.

(11) Takeuchi, K.; Yamamoto, N. Visualization of surface plasmon polariton waves in two-dimensional plasmonic crystal by cathodoluminescence. *Opt. Express* **2011**, *19*, 12365–12374.

(12) Ma, X.; Grüßer, M.; Schuster, R. Angular Dependence of Cathodoluminescence of Linear and Circular Au Gratings: Imaging the Coupling Angles between Surface Plasmon Polaritons and Light. *J. Phys. Chem. C* **2014**, *118*, 23247–23255.

(13) Sapienza, R.; Coenen, T.; Renger, J.; Kuttge, M.; van Hulst, N. F.; Polman, A. Deep-subwavelength imaging of the modal dispersion of light. *Nat. Mater.* **2012**, *11*, 781–787.

(14) van Wijngaarden, J.; Verhagen, E.; Polman, A.; Ross, C.; Lezec, H. J.; Atwater, H. A. Direct imaging of propagation and damping of near-resonance surface plasmon polaritons using cathodoluminescence spectroscopy. *Appl. Phys. Lett.* **2006**, *88*, 221111.

(15) Coenen, T.; Vesseur, E. J. R.; Polman, A.; Koenderink, A. F. Directional emission from plasmonic Yagi Uda antennas probed by angle-resolved cathodoluminescence spectroscopy. *Nano Lett.* **2011**, *11*, 3779–3784.

(16) Yamamoto, N.; Ohtani, S.; García de Abajo, F. J. Gap and Mie plasmons in individual silver nanospheres near a silver surface. *Nano Lett.* **2011**, *11*, 91–95.

(17) Gorodetski, Y.; Drezet, A.; Genet, C.; Ebbesen, T. W. Generating Far-Field Orbital Angular Momenta from Near-Field Optical Chirality. *Phys. Rev. Lett.* **2013**, *110*, 203906.

(18) Lu, L.; Joannopoulos, J. D.; Soljacic, M. Topological photonics. *Nat. Photonics* **2014**, *8*, 821–829.

(19) Onoda, M.; Murakami, S.; Nagaosa, N. Hall Effect of Light. *Phys. Rev. Lett.* **2004**, *93*, 083901.

(20) Yin, X.; Ye, Z.; Rho, J.; Wang, Y.; Zhang, X. Photonic Spin Hall Effect at Metasurfaces. *Science* **2013**, *339*, 1405–1407.

(21) Li, G.; Kang, M.; Chen, S.; Zhang, S.; Pun, E. Y.-B.; Cheah, K. W.; Li, J. Spin-Enabled Plasmonic Metasurfaces for Manipulating Orbital Angular Momentum of Light. *Nano Lett.* **2013**, *13*, 4148–4151.

(22) O'Connor, D.; Ginzburg, P.; Rodríguez-Fortuño, F. J.; Wurtz, G. A.; Zayats, A. V. Spin-orbit coupling in surface plasmon scattering by nanostructures. *Nat. Commun.* **2014**, 5.532710.1038/ncomms6327

(23) Coenen, T.; Polman, A. Polarization-sensitive cathodolumines-cence Fourier microscopy. *Opt. Express* **2012**, *20*, 18679–19691.

(24) Coenen, T.; Bernal Arango, F.; Koenderink, A. F.; Polman, A. Directional emission from a single plasmonic scatterer. *Nat. Commun.* **2014**, *5*, 3250.

(25) Fallet, C.; Novikova, T.; Foldyna, M.; Manhas, S.; Ibrahim, B. H.; Martino, A. D.; Vannuffel, C.; Constancias, C. Overlay measurements by Mueller polarimetry in back focal plane. *J. Micro/ Nanolithogr., MEMS, MOEMS* **2011**, *10*, 033017.

(26) Arteaga, O.; Maoz, B. M.; Nichols, S.; Markovich, G.; Kahr, B. Complete polarimetry on the asymmetric transmission through subwavelength hole arrays. *Opt. Express* **2014**, *22*, 13719–13732.

(27) Kruk, S. S.; Staude, M. D. I.; Schlecht, S.; Greppmair, M.; Neshev, D. N.; Kivshar, Y. S. Spin-Polarized Photon Emission by Resonant Multipolar Nanoantennas. *ACS Photonics* **2014**, *1*, 1218–1223.

(28) Osorio, C. I.; Mohtashami, A.; Koenderink, A. F. K-space polarimetry of bullseye plasmon antennas. *Sci. Rep.* **2015**, *5*, 9966.

(29) Coenen, T.; Vesseur, E. J. R.; Polman, A. Angle-resolved cathodoluminescence spectroscopy. *Appl. Phys. Lett.* **2011**, *99*, 143103.

(30) Lieb, M.; Zavislan, J.; Novotny, L. Single-molecule orientations determined by direct emission pattern imaging. *J. Opt. Soc. Am. B* **2004**, *21*, 1210–1215.

(31) Kosako, T.; Kadoya, Y.; Hofmann, H. F. Directional control of light by a nano-optical Yagi-Uda antenna. *Nat. Photonics* **2010**, *4*, 312–315.

(32) Curto, A. G.; Volpe, G.; Taminiau, T. H.; Kreuzer, M.; Quidant, R.; van Hulst, N. F. Unidirectional emission of a quantum dot coupled to a nanoantenna. *Science* **2010**, *329*, 930–933.

(33) Aouani, H.; Mahboub, O.; Bonod, N.; Devaux, E.; Popov, E.; Rigneault, H.; Ebbesen, T. W.; Wenger, J. Bright unidirectional fluorescence emission of molecules in a nanoaperture with plasmonic corrugations. *Nano Lett.* **2011**, *11*, 637–644.

(34) Sersic, I.; Tuambilangana, C.; Koenderink, A. F. Fourier microscopy of single plasmonic scatterers. *New J. Phys.* **2011**, *13*, 083019.

(35) Belacel, C.; Habert, B.; Bigourdan, F.; Marquier, F.; Hugonin, J. P.; Michaelis de Vasconcellos, S.; Lafosse, X.; Coolen, L.; Schwob, C.; Javaux, C.; Dubertret, B.; Greffet, J. J.; Senellart, P.; Maitre, A. Controlling spontaneous emission with plasmonic optical patch antennas. *Nano Lett.* **2013**, *13*, 1516–1521.

(36) Rodríguez-Herrera, O. G.; Bruce, N. C. Confined three-dimensional plasmon modes inside a ring-shaped nanocavity on a silver film imaged by cathodoluminescence microscopy. *Opt. Eng.* **2006**, *45*, 053602.

(37) Rodríguez-Herrera, O. G.; Rosete-Aguilar, M.; Bruce, N. C. Cambio del estado de polarización en un espejo elíptico. *Rev. Mex. Fis.* **2004**, *E50*, 33−40.

(38) Berry, H. G.; Gabrielse, G.; Livingston, A. E. Measurement of the Stokes parameters of light. *Appl. Opt.* **1977**, *16*, 3200−3205.

(39) Born, M.; Wolf, E. *Principles of Optics: Electromagnetic Theory of Propagation, Interference and Diffraction of Light*, 7th ed.; Cambridge University Press, 1997.

(40) Chipman, R. A. In *Handbook of Optics, Geometrical and Physical Optics, Polarized Light, Components and Instruments*, 3rd ed.; Bass, M., DeCusatis, C., Enoch, J., Lakshminarayanan, V., Li, G., Macdonald, C., Mahajan, V., Van Stryland, E., Eds.; McGraw-Hill, Inc.: New York, NY, 2010; Vol. *I*.

(41) Lezec, H. J.; Degiron, A.; Devaux, E.; Linke, R. A.; Martín-Moreno, L.; Garcia-Vidal, F. J.; Ebbesen, T. W. Beaming light from a subwavelength aperture. *Science* **2002**, *297*, 820−822.

(42) Jun, Y. C.; Huang, K. C. Y.; Brongersma, M. L. Plasmonic beaming and active control over fluorescent emission. *Nat. Commun.* **2011**, *2*, 283.

(43) Han, S.; Norris, D. Beaming thermal emission from hot metallic bull's eyes. *Opt. Express* **2010**, *18*, 4829−4837.

(44) Kuttge, M.; Vesseur, E. J. R.; Koenderink, A. F.; Lezec, H. J.; Atwater, H. A.; García de Abajo, F. J.; Polman, A. Local density of states, spectrum, and far-field interference of surface plasmon polaritons probed by cathodoluminescence. *Phys. Rev. B: Condens. Matter Mater. Phys.* **2009**, *79*, 113405.

(45) Rui, G.; Abeysinghe, D. C.; Nelson, R. L.; Zhan, Q. Demonstration of beam steering via dipole-coupled plasmonic spiral antenna. *Sci. Rep.* **2013**, *3*, 2237.

(46) Mohtashami, A.; Coenen, T.; Antoncecchi, A.; Polman, A.; Koenderink, A. F. Nanoscale excitation mapping of plasmonic patch antennas. *ACS Photonics* **2014**, *1*, 1134.

(47) Drezet, A.; Genet, C.; Laluet, J.-Y.; Ebbesen, T. W. Optical chirality without optical activity:How surface plasmons give a twist tolight. *Opt. Express* **2008**, *16*, 12559−12570.

(48) Rui, G.; Chen, W.; Abeysinghe, D. C.; Nelson, R. L.; Zhan, Q. Beaming circularly polarized photons from quantum dots coupled with plasmonic spiral antenna. *Opt. Express* **2012**, *20*, 19297−19304.

(49) Rui, G.; Nelson, R. L.; Zhan, Q. Circularly polarized unidirectional emission via a coupled plasmonic spiral antenna. *Opt. Lett.* **2011**, *36*, 4533−4535.

(50) Brenny, B. J. M.; Coenen, T.; Polman, A. Quantifying coherent and incoherent cathodoluminescence in semiconductors and metals. *J. Appl. Phys.* **2014**, *115*, 244307.